Journal of Alloys and Compounds 509 (2011) 326–331

Contents lists available at ScienceDirect

Journal of Alloys and Compounds

journal homepage: www.elsevier.com/locate/jallcom

Effects of annealing temperature, atomic composition, film thickness on structure and magnetic properties of CoPt composite films

Y.J. Zhang[a,b], Y.T. Yang[a,b], Y. Liu[a,b], Y.X. Wang[a,b], X.Y. Li[a,b], D.D. Wang[c], J. Cao[c], N.N. Yang[a,b], J. Li[a,b], S.Y. Yang[a,b], Y.Q. Liu[a,b], M.B. Wei[a,b], J.H. Yang[a,b,*]

[a] Institute of Condensed State Physics, Jilin Normal University, Siping 136000, People's Republic of China
[b] Key Laboratory of Functional Materials Physics and Chemistry (Jilin Normal University), Ministry of Education, Siping 136000, People's Republic of China
[c] Key Laboratory of Excited State Processes, Changchun Institute of Optics, Fine Mechanics and Physics, Chinese Academy of Sciences, Changchun 130033, People's Republic of China

ARTICLE INFO

Article history:
Received 1 April 2010
Received in revised form 29 August 2010
Accepted 1 September 2010
Available online 21 September 2010

Keywords:
$L1_0$ phase
Phase transformation
Magnetization reversal mechanism

ABSTRACT

$L1_0$–CoPt was obtained by annealing the CoPt film at 600 °C after co-sputtering Co and Pt targets in a magnetron sputtering system. X-ray diffraction (XRD) and high-resolution transmission electron microscopy (HRTEM) results showed a transformation from the face-centered-cubic (FCC) structure to the $L1_0$ ordered structure during the post-deposition annealing. Thermal stress (S_T), intrinsic stress (S_i) and total stress (S_{total}) in the films decreased with the increase of the annealing temperature. When the Co atomic composition was 50%, the coercivity of the CoPt film reached to a giant value, around 6300 Oe. The stress was released when the film thickness increased. The relaxed residual stress accounted for the enhancement in the coercivity. Magnetization reversal mechanism of the $Co_{50}Pt_{50}$ film followed neither the S–W model nor the DWM model.

1. Introduction

Considerable attention has recently been given to $L1_0$ structured CoPt and FePt films [1–6] and their nanoparticles [7,8] because of their potential applications in future ultrahigh-density magnetic-storage media. Due to the large surface/volume ratio, nanoparticles oxidize easily in air and form oxides that tend to be typically antiferromagnetic [9]. The existence of impurities also complicates the observations on the structure transformation, and further on the magnetism [10]. Compared to FePt alloys, CoPt alloy films exhibit a better oxidation and corrosion resistance [11], which makes $L1_0$ CoPt more suitable for the ultrahigh-density recording.

In general, the random distribution of the atoms in the as-deposited CoPt films results in a disordered FCC structure and soft ferromagnetic properties [12]. The associated hard magnetic ordered $L1_0$ face-centered-tetragonal (FCT) phase can be obtained by annealing at moderately high temperature and the high magnetic anisotropy strongly correlates with the long-range order parameter of the $L1_0$ structure [1,3,6,13–15]. However, when the growth temperature increases, the considerable particle coalescence leads to the increased switching volumes, which defeats the point of making small particles [16]. A significant reduction of the ordering temperature can be achieved by doping Sn, Pb, Sb, Bi, Ge or Ag into the sputtered films [2–6], but the doping process is not well controlled and the doping will increase the probability of the impurities appearance, which makes the material unsuitable for the practical applications. Therefore, some researchers attempt to improve its magnetic properties by adjusting the ratio of Co and Pt composition [17,18]. Recently, metastable phase $L1_1$ CoPt thin film attracts considerable interests because of the high K_u, low formation temperature (less than 300 °C) and good chemical stability [19]. However, the order parameter (S) is below 0.5, which is urgently needed to be improved for optimizing the $L1_1$ phase [20].

It is worthy of note that the stress can arise from various sources such as the different coefficient of thermal expansion (CTE), the lattice mismatch between substrate and film layer, the residual stress of the as-deposited films, the volume shrinkage during phase transformation and the grain growth during the annealing process [3,21–23]. Stress is not only effective to induce the texture in the $L1_0$–CoPt films, but also lead to the distortion of the lattice of the films, which may have a great impact on the magnetic properties of the materials [24]. In addition, the order parameter of the film often varies when the ratio of Co and Pt composition changes. However, there is no simple correlation between the film anisotropy constant and the order parameter [25,26]. Hence, it is still important to understand the relations between the order parameter and the magnetic property. Last but not least, the coercivity of the film is mainly determined by the magnetic reversal mechanism, including nucleation in SmFeN permanent magnets [27], domain wall motion in Nb-poor Finemet-type alloys [28], and

* Corresponding author at: Institute of Condensed State Physics, Jilin Normal University, No. 1301, Haifeng Street, Siping 136000, People's Republic of China.
Tel.: +86 434 3294566.
E-mail address: jhyang1@jlnu.edu.cn (J.H. Yang).

0925-8388/$ – see front matter © 2010 Elsevier B.V. All rights reserved.
doi:10.1016/j.jallcom.2010.09.020

Stoner–Wohlfarth (S–W) behavior in small particles [29]. Therefore, it is necessary to analyze coercivity mechanism of the CoPt films by combining the experimental data with the theoretical studies. More detailed investigations of the CoPt films are urgent to explore the nature of this material for the sake of the applications in the near future.

In this work, we systematically investigate the effects of the annealing temperature, stress, Co composition, order parameter (S) and film thickness on structure and magnetic properties of the CoPt composite films. In addition, the magnetization reversal mechanism of the $Co_{50}Pt_{50}$ film is discussed in detail.

2. Experimental details

The CoPt films are deposited by co-sputtering pure Co and Pt targets on Si substrate in the ATC 1800F sputtering system at the ambient temperature, under an ultra pure Ar environment (99.999%). The deposition power is fixed at about 20 W for Pt, and the Co deposition power is varied in the nominal range of 40–60 W. The chemical composition is controlled by varying Co deposition power. The base pressure of the chamber is below 3×10^{-7} Torr. The sputtering gas is Ar and the sputtering pressure is maintained at 5 mTorr. After deposition, the films are post-annealed at various temperatures from 0 to 600 °C in high vacuum (10^{-6} Torr) and the annealing time is 30 min.

Crystal structure and residual stress analysis of the CoPt films are characterized by XRD on D/max-2500 copper rotating-anode X-ray diffractometer with Cu Kα radiation (40 kV, 200 mA). The stress in the film is evaluated from the slope data obtained by $\sin^2\psi$ method. A slow scanning speed of 1 °/min is used to differentiate the two peaks; $L1_0$ (1 1 1) and FCC (1 1 1). Magnetic properties are measured by a Lake Shore 7407 vibrating sample magnetometer (VSM). The chemical composition is determined by the X-ray Fluorescence (XRF ZSX Primus II) measurements. The microstructure and the interplanar distance of the films are investigated by HRTEM (200 keV, JEM-2100HR).

3. Results and discussion

3.1. Effect of annealing on the disorder–order transformation

Fig. 1(a) shows the XRD patterns for the $Co_{44}Pt_{56}$ films (100 nm) annealed in high vacuum at different temperatures for 30 min. When annealed below 500 °C, the CoPt films show the fundamental peaks associated with (1 1 1) and (2 0 0), indicating the disordered FCC structure. The low peak intensities imply the poor crystallization. As the annealing temperature increases to 600 °C, the superlattice peaks of (0 0 1) and (1 1 0) appear, and the peak (2 0 0) broadens and eventually splits into two peaks corresponding to FCC (2 0 0) and FCT (0 0 2), which reveals the disorder–order phase transformation from the FCC to the $L1_0$-ordered FCT.

The stress relaxation is an important factor to control the structure, magnetic and electronic properties of the films [30,31]. According to Rasmussen's report [32], the thermal stress (S_T) versus the annealing temperature relationship is given by

$$S_T = \Delta a \quad \Delta T \left\{ \frac{E}{(1-\upsilon)} \right\}, \tag{1}$$

where $\Delta\alpha$ is the difference between the CTE of the substrate and the magnetic film; ΔT is the change in temperature between room temperature and annealing temperature; E is the elastic modulus of the film and υ is the Poisson's ratio. The material constants we used in the calculations are listed below:

CTE: $\alpha_{Si(100)} = 8.2 \times 10^{-6}\ K^{-1}$, $\alpha_{CoPt} = 10.9 \times 10^{-6}\ K^{-1}$.
Elastic modulus: $E_{CoPt} = 188$ GPa.
Poisson's ratio: $\upsilon_{CoPt} = 0.33$ [31,32].

The intrinsic stress (S_i) is a function of the slope of $\sin^2\psi$ method (P), Poisson's ratio (υ) and Young's modulus (E):

$$S_i = \frac{PE}{2(1+\upsilon)} \cot\theta, \tag{2}$$

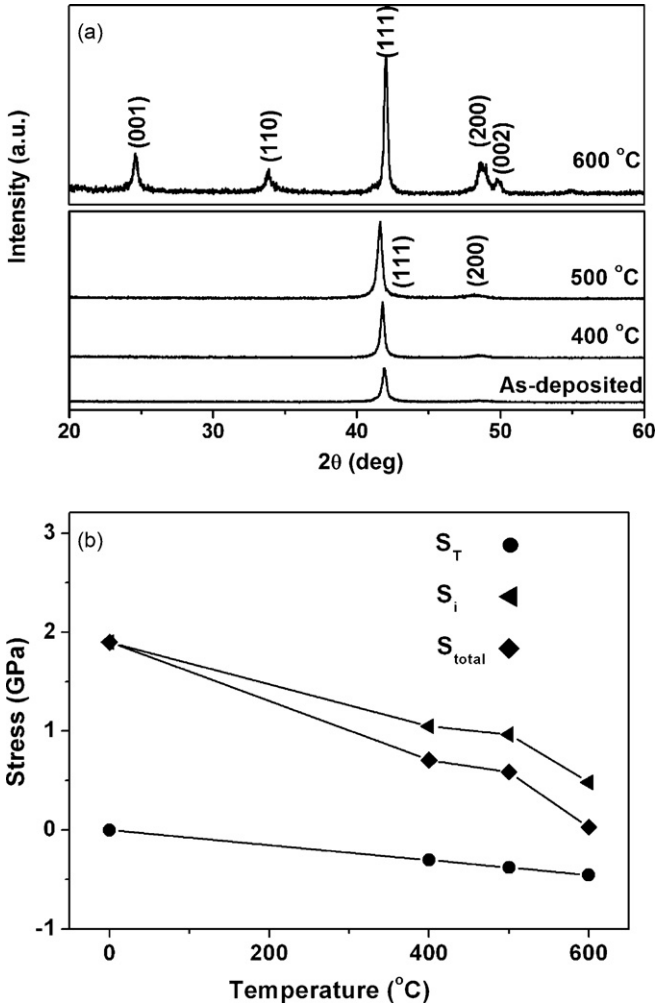

Fig. 1. (a) XRD patterns of the $Co_{44}Pt_{56}$ films annealed at various temperatures and (b) Dependence of S_{total}, S_i and S_T on the annealing temperature for the $Co_{44}Pt_{56}$ films.

where θ is the angle of the studied diffraction peak [33]. For both S_T and S_i, a negative value means that the film is in compression, while a positive value means a tensile stress.

Fig. 1(b) shows the dependence of S_T, S_i and S_{total} (S_T plus S_i) on the annealing temperature. The calculations indicate that S_T exists as a compressive stress while S_i is a tensile one. S_T, S_i and S_{total} in the film decrease with the increase of the temperature. Tensile stress occurs and is relaxed by the formation of microtwins due to the lattice mismatch between substrate and film [34]. Stress is considered to be effective to influence texture in the $L1_0$–MPt (M = Co and Fe) films [3,6,22,24]. We believe that the relaxation mechanism of the stress may favor the formation of the $L1_0$–CoPt.

Fig. 2(a) and (b) presents the energy dispersive spectroscopy (EDS) spectrum and HRTEM image of the $Co_{44}Pt_{56}$ film annealed at 600 °C for 30 min, respectively. The survey scans show the existence of the Co and Pt ions in the CoPt film and no impurity is detected within the detection limit. The Cu peak at about 8.05 keV and the C peak at about 0.30 keV come from copper grid. HRTEM micrograph shows the crystal lattice structure with different orientations. The measured interplanar distances of the fringes are 0.370, 0.269 and 0.218 nm, corresponding to the (0 0 1), (1 1 0) and (1 1 1) crystallographic planes of $L1_0$ CoPt, in agreement with the XRD results.

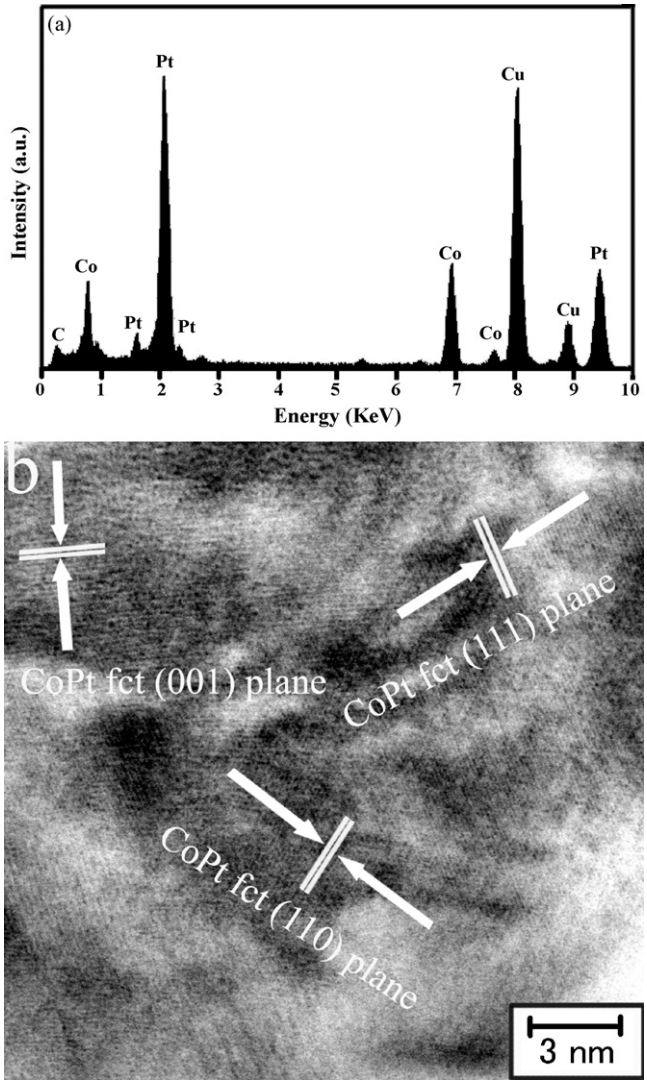

Fig. 2. (a) EDS spectrum and (b) HRTEM image of the $Co_{44}Pt_{56}$ film annealed at 600 °C.

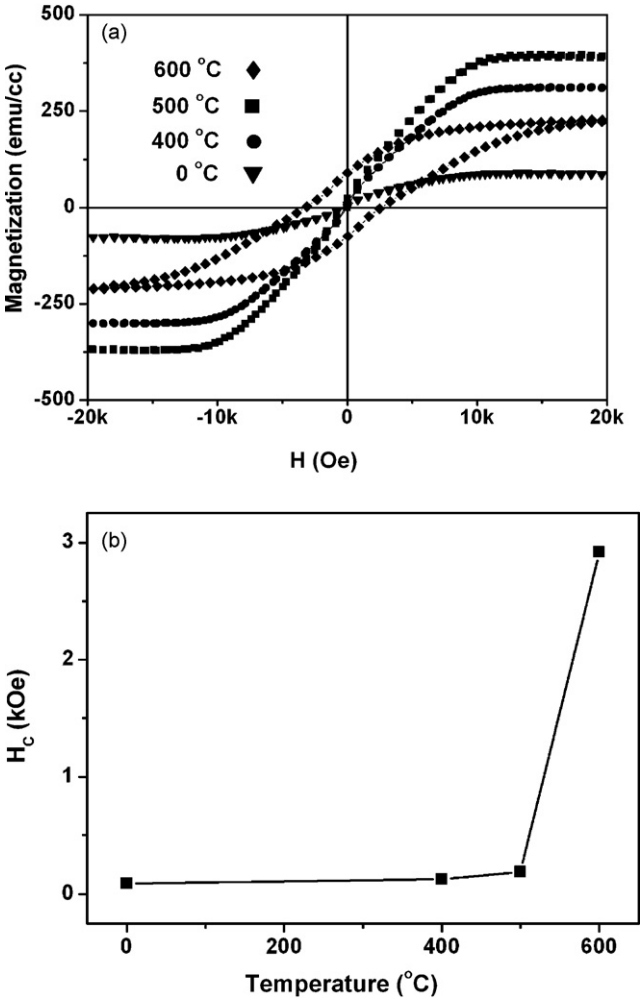

Fig. 3. (a) M–H loops of the $Co_{44}Pt_{56}$ films annealed at different temperatures and (b) the plot of H_C as a function of annealing temperature for the $Co_{44}Pt_{56}$ films.

In order to investigate the magnetic properties of the CoPt films, the perpendicular coercivity (H_C) is discussed. Fig. 3(a) shows the M–H curves of the $Co_{44}Pt_{56}$ films annealed at different temperatures. When the $Co_{44}Pt_{56}$ film is annealed below 500 °C, the saturation magnetization (M_S) increases continuously. The chemically ordered phase has a smaller moment than that of the disordered phase, which leads to the reduction in M_S. Therefore, when the annealing temperature is above 500 °C, M_S decreases because of the gradual phase transformation [9]. The effect of annealing temperature on coercivity is observed in Fig. 3(b). When the annealing temperatures are below 500 °C, the films dominantly show the FCC characteristics with the H_C of a few hundred Oe. The FCC phase has a low magnetocrystalline anisotropy and gives small coercivity. When the annealing temperatures are beyond 500 °C, the film becomes magnetically harder, and H_C increases considerably because of the formation of the ordered $L1_0$ phase. H_C of the film annealed at 600 °C is about 3200 Oe, indicating the transformation from the FCC to the FCT phase, which is consistent with the emergence of the superlattice (0 0 1), (1 1 0) and (0 0 2) peaks of CoPt shown in the XRD results. Toney et al. reported that the volume averaged chemical order (S_{ave}) increased and growth faults decreased as the growth temperature increased [35]. In addition, Barmak et al. reported that the structure and width of the magnetic domains of CoPt films demonstrated an increase in magnetic anisotropy when the deposition temperature increased [25]. These interpretations may also be responsible for the changes of coercivity in our samples. In order to avoid coalescence and to obtain reasonably large CoPt grains, 600 °C is chosen for the growth temperature in the following investigations.

3.2. Effect of Co composition on structure and magnetic properties

To further understand the structure and magnetic properties of these CoPt films, it is essential to investigate CoPt films with controlled composition. Fig. 4 shows the XRD patterns of the Co_xPt_{100-x} (x = 40, 44, 48, 50, 52) films annealed at 600 °C for 30 min. The chemical composition of the CoPt film is determined by the XRF measurements (not shown here). $Co_{40}Pt_{60}$ exhibits the poor crystalline quality with the presence of (1 1 0), (1 1 1) and (2 0 0) peaks. When Co composition is over 44%, the peaks corresponding to the $L1_0$ CoPt (0 0 1), (1 1 0), (1 1 1) and (0 0 2) diffractions appear. With increasing Co composition, the peaks show the gradual shift to the high angle. It is well known that Pt atom is larger in size than that of Co atom. Therefore, the cell parameter decreases when the larger Pt atom is replaced by the smaller Co atom. Among all these films, $Co_{50}Pt_{50}$ possesses a good crystalline

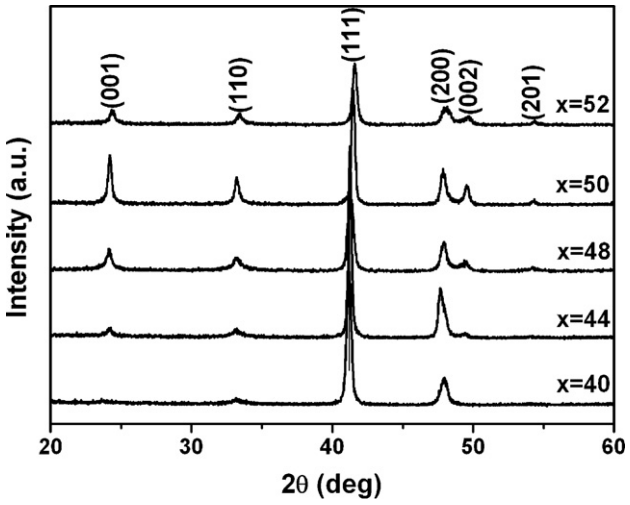

Fig. 4. XRD patterns of the Co_xPt_{100-x} films (x = 40, 44, 48, 50, 52).

structure. $Co_{50}Pt_{50}$ gives c/a = 0.974, which is almost the same as that of $L1_0$ CoPt alloys [11].

Fig. 5(b) shows the dependence of S and H_C on Co composition for the 100 nm CoPt films. S (definition reported in Ref. [6,14,36–38]) of Co_xPt_{100-x} (x = 40, 44, 48, 50, 52) is calculated about 0.27, 0.49, 0.73, 0.82 and 0.60, respectively. H_C is calculated from the corresponding curves of M–H in Fig. 5(a). The maximum H_C (6350 Oe) is obtained around the equiatomic composition. The

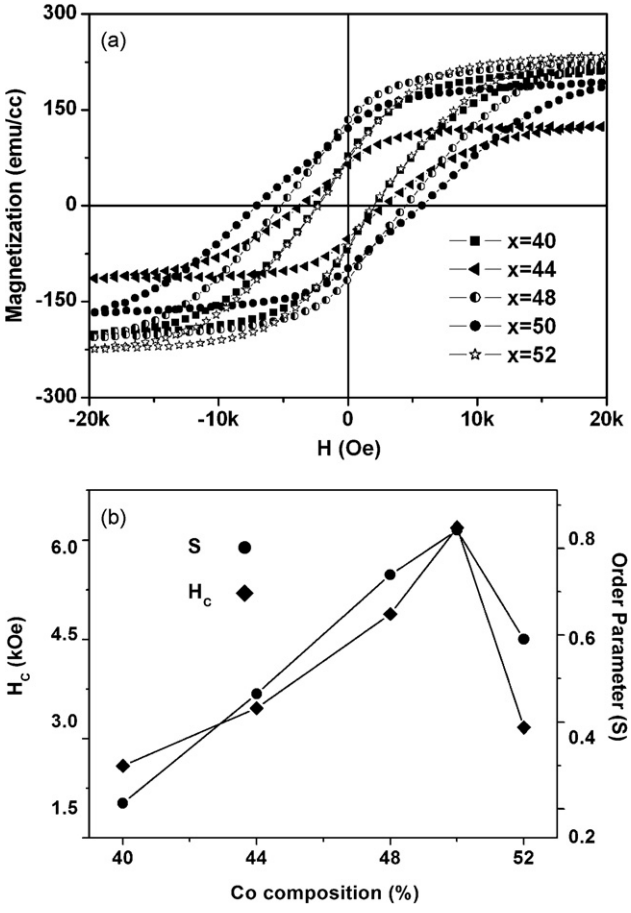

Fig. 5. (a) M–H loops of the Co_xPt_{100-x} films (x = 40, 44, 48, 50, 52) at room temperature under 20 kOe and (b) dependence of H_C and S on Co composition.

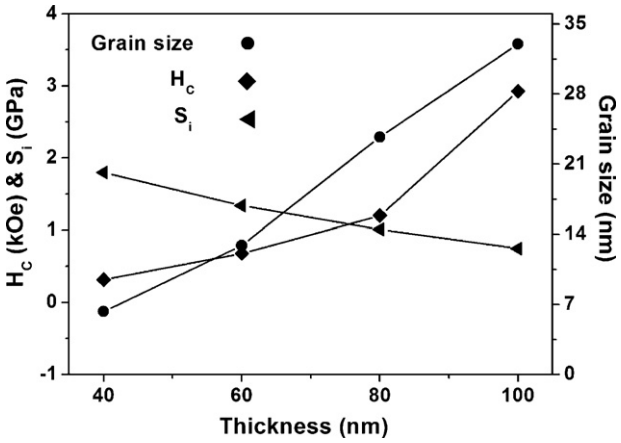

Fig. 6. Dependence of grain size, H_C and S_i of $\sin^2\psi$ method on film thickness.

H_C value is similar to that of Ref. [39], and higher than that of the nanoparticles reported by other researchers [40,41]. The differences of H_C between nanoparticles and films can be ascribed to the different kinetic and thermodynamic behavior of the ordering process [1,7,14,42–45]. Since the coercivity is closely related to the magnetocrystalline anisotropy of an individual grain [25], the different Co compositions will result in different magnetocrystalline anisotropies and H_C. The changes in the order parameter with Co composition may be the possibility for H_C variations. Furthermore, Razee et al. reported that the compositional order enhanced the magnitude of magnetocrystalline anisotropy energy (MAE) by some two orders in the $Co_{50}Pt_{50}$ alloy [46], which might be responsible for the high H_C of $Co_{50}Pt_{50}$. Present result on $Co_{50}Pt_{50}$ films are inconsistent with the previous ones [25,26], in which the highest anisotropies are found for compositions that are slightly Co rich. Detailed studies on anisotropy dependence of Co composition are in progress.

3.3. Effect of residual stress on magnetic properties

Fig. 6 shows the dependence of the grain size, H_C, and S_i on film thickness. The $Co_{50}Pt_{50}$ films are annealed at 600 °C for 30 min and the thickness is about 100, 80, 60, 40 nm, respectively. We do not show the M–H curves. The grain size is estimated by Scherrer's formula using the (1 1 1) peak width from the XRD patterns. The mean grain size is about 6.3, 12.9, 23.7 and 33 nm for the film thickness 40, 60, 80 and 100 nm, respectively. For the $Co_{50}Pt_{50}$ films, the variation of H_C is similar to the variation of grain size within the film thickness 40–100 nm. By the $\sin^2\psi$ method mentioned above, S_i is calculated to be positive, indicating a tensile stress in the $Co_{50}Pt_{50}$ films. And the tensile stress is released when the film thickness increases as shown in Fig. 6. The relaxed tensile stress can account for the enhancement in the coercivity of the $Co_{50}Pt_{50}$ films [33]. The results can satisfactorily explain the increase in H_C with thickness. In addition, both the order parameter and the fault spacing increase with increasing film thickness, which may be responsible for the increment of H_C [14,35].

3.4. Magnetization reversal analysis

Fig. 7 shows the angular dependence of the coercivities H_C (θ) obtained for the $Co_{50}Pt_{50}$ film annealed at 600 °C and the film thickness is 40 nm. The angular dependence of coercivity with different applied field is measured and normalized to the respective coercivity at θ = 0°, where θ is the angle between the applied field and the film easy axis or plane. In the ideal S–W model [29],

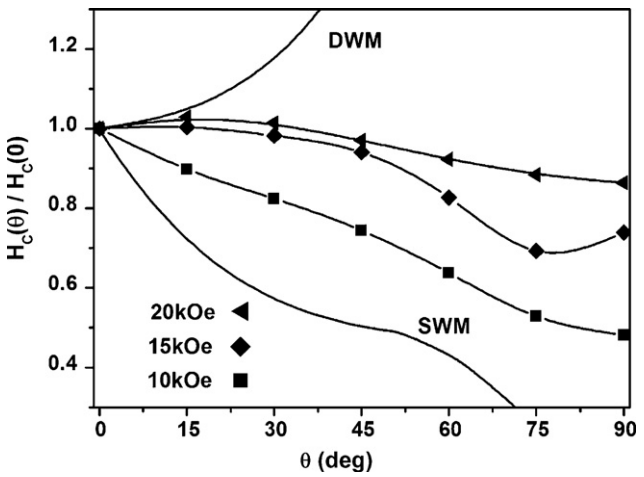

Fig. 7. Angular dependence of normalized coercivity ($H_C(\theta)/H_C(0)$) for the $Co_{50}Pt_{50}$ film annealed at 600 °C. The curves of S–W model and the DWM model are plotted for comparison. S–W indicates coherent switching in S–W model (SWM) particles and Domain wall motion (DWM) model following $1/\cos\theta$ indicates incoherent switching behavior.

the variation of coercivity upon θ obeys the function $H_C(\theta)/H_C(0) = (\cos^{2/3}\theta + \sin^{2/3}\theta)^{-3/2}$ for $\theta < 45°$ and $H_C(\theta)/H_C(0) = \sin\theta\cos\theta$ for $45° < \theta \leq 90°$. The function of DWM model [47], $H_C(\theta)/H_C(0) = 1/\cos\theta$ for $\theta \leq 90°$, is also plotted for comparison. When measured under the applied field 20, 15, 10 kOe, all $H_C(\theta)/H_C(0)$ curves show the decreases on a large angle range. In general, the angular variation $H_C(\theta)/H_C(0)$ shows a closer resemblance to the S–W model compared to the DWM model. However, when measured in 20 kOe field, $H_C(\theta)/H_C(0)$ increases slightly from 0° to 30°, decreases in the range of $30° < \theta < 90°$. When measured in 15 kOe applied filed, $H_C(\theta)/H_C(0)$ decreases gradually from 15° to 75° and increases from 0° to 15°, 75° to 90°. Therefore, the qualitative comparison indicates that magnetization reversal mechanism of the $Co_{50}Pt_{50}$ film follows neither the S–W model nor the DWM model due to the obvious lack of agreement between the experimental curves and the theoretical curves. Jeong et al. reported the possibilities of both domain wall motion and rotational mechanism for the $L1_0$ CoPt polycrystalline films [48]. In addition, it is found that the magnetization reversal in polycrystalline $L1_0$–FePt films was the nucleation-type [34]. Therefore, there is a possibility that several mechanisms co-exist, depending on the grain size and the complicated microstructures of the grains. Further analysis is necessary for a deep understanding of the reversal mechanism.

4. Conclusions

In summary, the magnetic CoPt films are successfully prepared by co-sputtering method at room temperature. The $L1_0$ ordered CoPt phase is obtained by adjusting the annealing temperature and Co composition. Thermal treatment induces the CoPt disorder–order phase transformation from the FCC to the $L1_0$-ordered FCT. HRTEM results further verify that $L1_0$–CoPt is obtained after annealing at 600 °C. The stress differences between the annealed and the as-deposited state indicate the changes of the film microstructure. S_T, S_i and S_{total} in the films decrease with the increase of the annealing temperature. The stress is released when the film thickness increases. The relaxed residual stress with thickness accounts for the enhanced coercivity. Magnetization reversal mechanism of the $Co_{50}Pt_{50}$ film is found to follow neither the S–W model nor the DWM model. Our work provides an effective way to enhance both structure and magnetic properties of the ordered $L1_0$ CoPt films, which will play an important role in prompting its practical applications in the future.

Acknowledgements

This work is supported by the National Programs for High Technology Research and Development of China (863) (No. 2009AA03Z303), the National Youth Program Foundation of China (Nos. 10804036 and 10904050), Program for the development of Science and Technology of Jilin province (Nos. 20090331, 20090531 and 20082112), the program for importing foreign technology and management talents into China (No. 20092200028), the Eleventh Five-Year Program for Science and Technology of Education Department of Jilin Province (Nos. 20090190, 20090426 and 20080150), Program for the master students' scientific and innovative research of Jilin Normal University (No. S09010108).

References

[1] R.J. Tang, W.L. Zhang, Y.R. Li, J. Alloys Compd. 496 (2010) 380.
[2] J.L. Tsai, H.T. Tzeng, G.B. Lin, B.F. Liu, J. Alloys Compd. 502 (2010) 456.
[3] J.L. Tsai, G.B. Lin, H.T. Tzeng, J. Alloys Compd. 487 (2009) 18.
[4] K.F. Dong, X.F. Yang, J.B. Yan, W.M. Cheng, X.M. Cheng, X.S. Miao, J. Alloys Compd. 476 (2009) 662.
[5] O. Kitakami, Y. Shimada, K. Oikawa, H. Daimon, F. Fukamichi, Appl. Phys. Lett. 78 (2001) 1104.
[6] J.L. Tsai, C.J. Hsu, J. Alloys Compd. 426 (1996) 426.
[7] S.S. Kalyan Kamal, P.K. Sahoo, L. Durai, P. Ghosal, S. Ram, Manivel Raj, J. Alloys Compd. 501 (2010) 297.
[8] W.H. Qi, Y.J. Li, S.Y. Xiong, S.T. Lee, Small (2010), doi:10.1002/smll.201000274.
[9] Y. Kobayashi, M. Horie, D. Nagao, Y. Ando, T. Miyazaki, M. Konno, Mater. Lett. 60 (2006) 2046.
[10] S.P. Gubin, Magnetic Nanoparticles, WILEY-VCH Verlag GmbH & Co. KGaA, Weinheim, 2009.
[11] N.I. Vlasova, G.S. Kandaurova, N.N. Shchegoleva, J. Magn. Magn. Mater. 222 (2000) 138.
[12] S.U. Jen, J. Alloys Compd. 234 (1996) 231.
[13] Q.F. Xiao, E. Brück, Z.D. Zhang, F.R. de Boer, K.H.J. Buschow, J. Alloys Compd. 336 (2004) 41.
[14] W.B. Mi, J.J. Shen, W.J. Lu, H.L. Bai, J. Alloys Compd. 503 (2010) 233.
[15] Q.F. Xiao, E. Brück, Z.D. Zhang, F.R. de Boer, K.H.J. Buschow, J. Alloys Compd. 364 (2004) 64.
[16] S.S. Kang, J.W. Harrell, D.E. Nikles, Nano Lett. 2 (2002) 1033.
[17] P. Moskovkin, M. Hou, J. Alloys Compd. 434–435 (2007) 550.
[18] A. Demortière, C. Petit, Langmuir 23 (2007) 8575.
[19] A.C. Sun, F.T. Yuan, J.H. Hsu, H.Y. Lee, Scripta Mater. 61 (2009) 713.
[20] F.T. Yuan, A.C. Sun, J.H. Hsu, Scripta Mater. 62 (2010) 762.
[21] E. Ahmed, M. Takahashi, H. Iwasaki, K.I. Ohshima, J. Alloys Compd. 473 (2009) 1.
[22] C.W. Hsu, S.K. Chen, W.M. Liao, F.T. Yuan, W.C. Chang, J.L. Tsai, J. Alloys Compd. 449 (2008) 52.
[23] J. Dvorak, Y.U. Idzerd, S.B. Ogale, S. Shinde, T. Wu, T. Venkatesan, R. Godfrey, R. Ramesh, J. Appl. Phys. 97 (2005) 10C102-1.
[24] E. Manios, D. Stamopoulos, I. Panagiotopoulos, D. Niarchos, J. Phys. Conf. Ser. 153 (2009) 012060–012061.
[25] K. Barmak, J. Kim, L.H. Lewis, K.R. Coffey, M.F. Toney, A.J. Kellock, J.U. Thiele, J. Appl. Phys. 98 (2005) 033904–033911.
[26] K. Barmak, J. Kim, L.H. Lewis, K.R. Coffey, M.F. Toney, A.J. Kellock, J.U. Thiele, J. Appl. Phys. 95 (2004) 7501.
[27] X.C. Kou, J. Alloys Compd. 281 (1998) 41.
[28] H.S. Liu, C.H. Yin, X.X. Miao, Z.D. Han, D.H. Wang, Y.W. Du, J. Alloys Compd. 466 (2008) 246.
[29] E.C. Stoner, E.P. Wohlfarth, Philos. Trans. R. Soc. Lond. A 240 (1948) 599.
[30] T. Wu, J.F. Mitchell, Appl. Phys. Lett. 86 (2005) 062502–062511.
[31] W.M. Liao, S.K. Chen, F.T. Yuan, C.W. Hsu, H.Y. Lee, J. Magn. Magn. Mater. 303 (2006) e243.
[32] P. Rasmussen, X. Rui, J.E. Shield, Appl. Phys. Lett. 86 (2005) 191915–191921.
[33] H.P. Klug, L.E. Alexande, X-ray Diffraction Procedures, second ed., Wiley, New York, 1974.
[34] N.H. Goo, G. Schütz, E. Arzt, Formation of hard magnetic L10-FePt/FePd monolayers from elemental multilayers, Max-Planck-Institut für Metallforschung, Stuttgart, 2007.
[35] M.F. Toney, W.Y. Lee, J.A. Hedstrom, Andrew Kellock, J. Appl. Phys. 93 (2003) 9902.
[36] J.L. Tsai, C.J. Hsu, J. Alloys Compd. 455 (2008) 87.
[37] A. Kulovits, J.M.K. Wiezorek, W.A. Soffa, W. Püschl, W. Pfeiler, J. Alloys Compd. 378 (2004) 285.
[38] B.E. Warren, X-ray Diffraction, Dover, New York, 1990.
[39] E. Agostinelli, S. Laureti, G. Varvaro, A. Generosi, B. Paci, V. Rossi-Albertini, G. Scavia, A.M. Testa, Mater. Sci. Eng. C 27 (2006) 1466.

[40] C.N. Chinnasamy, B. Jeyadevan, K. Shinoda, K. Tohji, J. Appl. Phys. 93 (2003) 7583.
[41] A.C.C. Yu, M. Mizuno, Y. Sasaki, H. Kondo, Appl. Phys. Lett. 81 (2002) 3768.
[42] L. Castaldi, K. Giannakopoulos, A. Travlos, D. Niarchos, S. Boukari, E. Beaurepaire, Nanotechnology 19 (2008) 085701–085711.
[43] B. Yang, M. Asta, O.N. Mryasov, T.J. Klemmer, R.W. Chantrell, Acta Mater. 54 (2006) 4201.
[44] K. Zhang, Z. Chen, F. Liu, G.C. Yang, J. Alloys Compd. 501 (2010) L4.
[45] T. Spassov, P. Solsona, S. Suriñach, M.D. Baró, J. Alloys Compd. 345 (2002) 123.
[46] S.S.A. Razee, J.B. Staunton, B. Ginatempo, E. Bruno, F.J. Pinski, Phys. Rev. B 64 (2001) 014411–014421.
[47] E. Kondorsky, J. Phys., second ed., Moscow, 1940.
[48] S. Jeong, Y.N. Hsu, D.E. Laughlin, M.E.M. Henry, IEEE Trans. Magn. 36 (2000) 2336.